

Time-dependent Density Matrix Renormalization Group Quantum Dynamics for Realistic Chemical Systems

Xiaoyu Xie,¹ Yuyang Liu,¹ Yao Yao,² Ulrich Schollwöck,^{3, 4, a)} Chungen Liu,^{1, b)} and Haibo Ma^{1, c)}

¹⁾*School of Chemistry and Chemical Engineering, Nanjing University, Nanjing 210023, China*

²⁾*Department of Physics and State Key Laboratory of Luminescent Materials and Devices, South China University of Technology, Guangzhou 510640, China*

³⁾*Department of Physics, Arnold Sommerfeld Center for Theoretical Physics (ASC), Fakultät für Physik, Ludwig-Maximilians-Universität München, München D-80333, Germany*

⁴⁾*Munich Center for Quantum Science and Technology (MCQST), Schellingstr. 4, München D-80799, Germany*

(Dated: 8 May 2022)

Electronic and/or vibronic coherence has been found by recent ultrafast spectroscopy experiments in many chemical, biological and material systems. This indicates that there are strong and complicated interactions between electronic states and vibration modes in realistic chemical systems. Therefore, simulations of quantum dynamics with a large number of electronic and vibrational degrees of freedom are highly desirable. Due to the efficient compression and localized representation of quantum states in the matrix-product state (MPS) formulation, time-evolution methods based on the MPS framework, which we summarily refer to as tDMRG (time-dependent density-matrix renormalization group) methods, are considered to be promising candidates to study the quantum dynamics of realistic chemical systems. In this work, we benchmark the performances of four different tDMRG methods, including global Taylor, global Krylov, local one-site and two-site time-dependent variational principle (1TDVP and 2TDVP), with a comparison to multi-configuration time-dependent Hartree (MCTDH) and experimental results. Two typical chemical systems of internal conversion and singlet fission are investigated, one containing strong and high-order local and non-local electron-vibration couplings, the other exhibiting a continuous phonon bath. The comparison shows that the tDMRG methods (particularly, the 2TDVP method) can describe the full quantum dynamics in large chemical systems accurately and efficiently. Several key parameters in the tDMRG calculation including the truncation error threshold, time interval and ordering of local sites were also investigated to strike the balance between efficiency and accuracy of results.

^{a)}Electronic mail: schollwoeck@lmu.de

^{b)}Electronic mail: cgliu@nju.edu.cn

^{c)}Electronic mail: haibo@nju.edu.cn

I. INTRODUCTION

Solving the time-(in)dependent Schrödinger equation of a given non-relativistic quantum system is the most straightforward and commonly pursued idea to study its static properties and out-of-equilibrium behavior. Unfortunately, it is almost impossible to obtain exact solutions for large systems as the dimension of the configuration space grows exponentially with increasing system sizes. To tackle this so-called curse of dimensionality, many theoretical methods using different approximations have been proposed. Among them, tensor product methods^{1,2} recently attracted a lot of research interest. They treat quantum states and operators, expressed in products of local bases, as high-order tensors with an exponentially increasing number of coefficients and decompose these high-order tensors by different algorithms into suitable products of many low-rank and localised low-order tensors to compress the wave function and reduce the computational costs. One well-known decomposition algorithm is Tucker decomposition³ used in multi-configuration time-dependent Hartree (MCTDH)^{4,5}, which decomposes a high-order tensor with high rank into a set of matrices and one small Tucker core tensor with the same order but low rank; it can be considered as a high-order single value decomposition (HOSVD)^{6,7}. For higher orders, the Tucker core still suffers from the curse of dimensionality. This can be overcome by introducing multi-layer MCTDH (ML-MCTDH)⁸ using a hierarchical Tucker (HT) decomposition. The tensor train decomposition⁹ (TT; in the mathematical literature) or the equivalent matrix product state representation (MPS; in the physical literature)^{10,11} used in the density matrix renormalization group (DMRG)^{12,13} provide an alternative decomposition algorithm, which decomposes a high-order tensor with high rank into a product of many local low-order tensors with a one-dimension (1D) topology. This decomposition method has been generalized to tensor network states (TNS) such as projected entangled-pair states (PEPS)^{10,14} or tensor tree networks (TTN)^{15–18} for non-1D systems.

Among various tensor product methods, DMRG has been widely recognized as the most accurate numerical tool for calculating 1D strongly correlated systems, because of its two advantages of an efficient compression and a localized structure of its underlying MPS/TT formulation of the wave function. Following the success of DMRG in describing equilibrium quantities, various time-dependent variants (which we globally refer to by tDMRG) have been developed over the last 15 years, extending MPS/TT/DMRG to explore the real-time quantum dynamics of strongly correlated systems by solving the time-dependent Schrödinger equation (TDSE). In 2004, White and

Feiguin¹⁹, Daley et al.²⁰ and Verstraete et al.²¹ proposed algorithms based on the time-evolving block decimation (TEBD) algorithm of Vidal^{22,23}. They all use a Suzuki-Trotter decomposition²⁴ of the Hamiltonian into its individual two-body terms. When these terms are local, their time-evolution propagation operator can be applied efficiently to the wavefunction in MPS format. Unfortunately, Trotterization is not easily applicable to Hamiltonians with long-range interactions, which appear in quasi-2D systems or quantum chemistry applications as well as system-bath problems, but only after the use of numerous time-consuming site-swapping operations (“swap gates”). In order to deal with such general Hamiltonians, one can implement global time integration solvers (e.g. Runge-Kutta^{25–27} and Krylov²⁸ approaches) for TDSE based on the compressed MPS wavefunction directly for tDMRG without explicitly constructing the time evolution propagator. To exploit the second advantage of a localised structure in MPS/TT/DMRG, local tDMRG methods, including local Krylov^{28,29} and time-dependent variational principle (TDVP)^{30–32} approaches, were also developed, which solve a sequence of localised effective differential equations for time-evolution by introducing appropriate projectors of MPS/TT and inserting the projectors into the original TDSE. Moreover, the MPS/TT structure in tDMRG has also been successfully implemented in describing the mean-field operators and reduced/auxiliary density operators in MCTDH³³ and hierarchical equations of motion (HEOM)³⁴ simulations, and the grid-based wavepacket in split-operator Fourier transform (SOFT)³⁵ very recently.

In the last few years, tDMRG methods have been applied successfully for realistic chemical systems with electron-vibration (electron-phonon) interactions. Some of us implemented a unitary transformation approach for realistic vibronic Hamiltonians and simulated the charge transfer dynamics and 2D electronic spectrum of the oligothiophene/fullerene interface in organic solar cells via TEBD methods.³⁶ Shuai and coworkers simulated the absorption and fluorescence spectra of perylene bisimide (PBI) and distyrylbenzene molecular aggregates at zero and finite temperature by tDMRG methods using the fourth-order Runge-Kutta method combined with the thermofield dynamics approach²⁶. The TDVP methods were used by Reiher and coworkers³⁷ for the real- and imaginary-time evolution of PBI, pyrazine and ethylene systems containing a large number of degrees of freedom. Very recently, the TDVP approach was optimized by Ren and coworkers³⁸ with the help of graphical processing units (GPU) and multi-core central processing units (CPU); calculations of excitation energy transfer in FMO systems were found to be accelerated by a factor of up to 57 by using GPUs. These studies suggest the great potential of tDMRG methods for exploring the quantum dynamics of large chemical systems.

In order to provide practical guidelines for the future applications of various tDMRG methods in simulating the realistic chemical systems, in this work, we benchmark four different tDMRG methods (global Taylor, global Krylov, one-site and two-site TDVP) for two different chemical systems and compare our results with MCTDH, ML-MCTDH and experimental results. In Section II, we give a brief introduction to the framework of MPS and matrix product operators (MPO) (Section II A 1), global and local tDMRG methods (Section II A 2), and a general model for the study of chemical systems with electronic-vibration/phonon interactions (Section II B). The computational details and calculation results of S_1/S_2 internal conversion in pyrazine and singlet fission in molecular dimer are given in Section III A and III B respectively. Section IV presents a summary of this work.

II. METHODOLOGY

As the details of DMRG and tDMRG have been discussed elsewhere^{11,28,39}, we only briefly introduce the basic ideas of tDMRG methods in section II A and show how they are implemented for the simulation of the quantum dynamics of realistic chemical system by introducing models for electron-vibration interaction in section II B.

A. tDMRG methods

1. MPS and MPO

A general quantum state with n local sites can be expressed as a linear combination of orthonormal configurations (in terms of the local basis $\{|\sigma_i\rangle\}$):

$$|\psi\rangle = \sum_{\{\sigma_i\}} c_{\sigma_1\sigma_2\cdots\sigma_n} |\sigma_1\sigma_2\cdots\sigma_n\rangle. \quad (1)$$

The set of coefficient $c_{\sigma_1\sigma_2\cdots\sigma_n}$ can be regarded as a high-dimension tensor, which can be decomposed to the tensor train (TT) structure.⁹ In physics language, the state can be reformulated as an MPS:

$$|\psi\rangle = \sum_{\{\sigma_i\}, \{\alpha_i\}} A_{1,\alpha_1}^{\sigma_1} A_{\alpha_1,\alpha_2}^{\sigma_2} \cdots A_{\alpha_{n-1},1}^{\sigma_n} |\sigma_1\sigma_2\cdots\sigma_n\rangle, \quad (2)$$

$$= \sum_{\{\sigma_i\}} \mathbf{A}^{\sigma_1} \mathbf{A}^{\sigma_2} \cdots \mathbf{A}^{\sigma_n} |\sigma_1\sigma_2\cdots\sigma_n\rangle. \quad (3)$$

The rank-3 tensor $A_{\alpha_{i-1}, \alpha_i}^{\sigma_i}$ ($\alpha_0 = \alpha_n = 1$) has two bond legs (α_{i-1}, α_i) and one physical leg (σ_i), the bond dimension $m = \max(\alpha_i)$ is related to the amount of entanglement in $|\psi\rangle$ and is decreased by various truncation procedures such as singular value decomposition (SVD). A^{σ_i} is a rank-2 subtensor (matrix) of $A_{\alpha_{i-1}, \alpha_i}^{\sigma_i}$ with two indexes α_{i-1} (row index) and α_i (column index) for each $|\sigma_i\rangle$ of local site i .

In particular, a tensor $L_{\alpha_{i-1}, \alpha_i}^{\sigma_i}$ ($R_{\alpha_{i-1}, \alpha_i}^{\sigma_i}$) is called a left (right) orthonormal tensor if it satisfies the following equations,

$$\sum_{\sigma_i, \alpha_{i-1}} L_{\alpha_{i-1}, \alpha_i}^{\sigma_i} (L_{\alpha_{i-1}, \alpha'_i}^{\sigma_i})^* = \delta_{\alpha_i \alpha'_i}, \quad (4)$$

$$\sum_{\sigma_i, \alpha_i} (R_{\alpha_{i-1}, \alpha_i}^{\sigma_i})^* R_{\alpha'_{i-1}, \alpha_i}^{\sigma_i} = \delta_{\alpha_{i-1} \alpha'_{i-1}}. \quad (5)$$

Due to the gauge transformation symmetry ($A^{\sigma_i} \rightarrow A^{\sigma_i} X^{-1}$, $A^{\sigma_{i+1}} \rightarrow X A^{\sigma_{i+1}}$) of MPS, each MPS can be rebuilt as a left (right) canonical MPS consisting only of left (right) orthonormal tensor components or a so-called mixed-canonical MPS,

$$|\psi\rangle = \sum_{\{\sigma_k\}} \mathbf{L}^{\sigma_1} \mathbf{L}^{\sigma_2} \dots \mathbf{M}^{\sigma_i} \dots \mathbf{R}^{\sigma_{n-1}} \mathbf{R}^{\sigma_n} |\sigma_1 \sigma_2 \dots \sigma_n\rangle, \quad (6)$$

$$= \sum_{\sigma_i, \alpha_{i-1}, \alpha_i} M_{\alpha_{i-1}, \alpha_i}^{\sigma_i} |\mathcal{L}_{\alpha_{i-1}}^{[1:i-1]}\rangle |\sigma_i\rangle |\mathcal{R}_{\alpha_i}^{[i+1:n]}\rangle \quad (7)$$

$|\mathcal{L}_{\alpha_{i-1}}^{[1:i-1]}\rangle$ ($|\mathcal{R}_{\alpha_i}^{[i+1:n]}\rangle$) are block configurations with the left (right) orthonormal basis, the site i with arbitrary tensor component $M_{\alpha_{i-1}, \alpha_i}^{\sigma_i}$ is called active site or orthogonality center.

Correspondingly, every operator expressed in the local basis set $\{|\sigma_1 \dots \sigma_n\rangle\}$ can be rewritten as a MPO:

$$\hat{O} = \sum_{\{\sigma_i\}, \{\sigma'_i\}, \{w_i\}} W_{1, w_1}^{\sigma_1, \sigma'_1} \dots W_{w_{n-1}, 1}^{\sigma_n, \sigma'_n} |\sigma_1 \dots \sigma_n\rangle \langle \sigma'_1 \dots \sigma'_n|, \quad (8)$$

where the local tensor component $W_{w_{i-1}, w_i}^{\sigma_i, \sigma'_i}$ ($w_1 = w_n = 1$) is a rank-4 tensor with two bond legs (w_{i-1}, w_i) and two physical legs (σ_i, σ'_i) acting on ket and bra states respectively.

For the framework of MPS, two operations are key, the overlap between two states (MPS) and the application of an operator (MPO) to a state (MPS).

The calculation of the overlap between two MPS is straightforward due to the orthonormality

of the basis,

$$\begin{aligned} \langle \psi' | \psi \rangle &= \sum_{\{\sigma'_i\}, \{\alpha'_i\}} \left(A_{1,\alpha'_1}^{\sigma'_1} A_{\alpha'_1,\alpha'_2}^{\sigma'_1} \cdots A_{\alpha'_{n-1},1}^{\sigma'_n} \right)^\dagger \langle \sigma'_1 \sigma'_2 \cdots \sigma'_n | \\ &\times \sum_{\{\sigma_i\}, \{\alpha_i\}} A_{1,\alpha_1}^{\sigma_1} A_{\alpha_1,\alpha_2}^{\sigma_2} \cdots A_{\alpha_{n-1},1}^{\sigma_n} | \sigma_1 \sigma_2 \cdots \sigma_n \rangle \end{aligned} \quad (9)$$

$$= \sum_{\{\sigma_i\}} (\mathbf{A}'^{\sigma_n})^\dagger \cdots (\mathbf{A}'^{\sigma_1})^\dagger \mathbf{A}^{\sigma_1} \cdots \mathbf{A}^{\sigma_n}. \quad (10)$$

For an efficient evaluation, the final expression has to be evaluated in a suitable order; see e.g.¹¹.

The application of an MPO to an MPS can be carried out directly or variationally.

1. The direct procedure consists of straightforward tensor contractions between the local components of the MPS and the MPO,

$$\begin{aligned} \hat{O}|\psi\rangle &= \sum_{\{\sigma_i\}, \{\sigma'_i\}, \{w_i\}} W_{1,w_1}^{\sigma_1,\sigma'_1} \cdots W_{w_{n-1},1}^{\sigma_n,\sigma'_n} | \sigma_1 \cdots \sigma_n \rangle \langle \sigma'_1 \cdots \sigma'_n | \\ &\times \sum_{\{\sigma''_i\}, \{\alpha_i\}} A_{1,\alpha_1}^{\sigma''_1} \cdots A_{\alpha_{n-1},1}^{\sigma''_n} | \sigma''_1 \cdots \sigma''_n \rangle \end{aligned} \quad (11)$$

$$= \sum_{\{\sigma_i\}, \{w_i, \alpha_i\}} A_{1,w_1,\alpha_1}^{\sigma_1} \cdots A_{w_{n-1},\alpha_{n-1},1}^{\sigma_n} | \sigma_1 \cdots \sigma_n \rangle, \quad (12)$$

with the new tensor components $A_{w_{i-1},\alpha_{i-1},w_i,\alpha_i}^{\sigma_i}$ given by

$$A_{w_{i-1},\alpha_{i-1},w_i,\alpha_i}^{\sigma_i} = \sum_{\sigma'_i} W_{w_{i-1},w_i}^{\sigma_i,\sigma'_i} A_{\alpha_{i-1},\alpha_i}^{\sigma'_i} \quad (13)$$

2. The variational procedure approximates the result by minimizing the distance between the sought-for resulting MPS $|\phi\rangle$ and the MPO applied to the initial MPS,

$$\min_{|\phi\rangle} \| |\phi\rangle - \hat{O}|\psi\rangle \|^2. \quad (14)$$

By optimizing each local component $A_{\alpha_{i-1},\alpha_i}^{\sigma_i}$ of $|\phi\rangle$ and sweeping sites until convergence, the minimization in (14) is achieved, resulting in $|\phi\rangle$.

2. Time-evolution in the MPS framework: tDMRG methods

To solve the time-dependent Schrödinger equation (TDSE) and perform the time-evolution of a quantum state $|\psi(t)\rangle$, we can define the propagation operator $\hat{U}(t, t + \delta t)$

$$\hat{U}(t, t + \delta t) = e^{-i\hat{H}(t)\delta t/\hbar}, \quad (15)$$

such that the state is updated in time as

$$|\psi(t + \delta t)\rangle = \hat{U}(t, t + \delta t)|\psi(t)\rangle. \quad (16)$$

There are many ways to solve the TDSE by constructing the propagator \hat{U} (such as by a Taylor expansion, by diagonalizing the Hamiltonian or by Chebyshev methods⁴⁰, etc.) or by updating the state without explicit construction of \hat{U} (e.g. Runge-Kutta methods, Krylov subspace methods^{41,42} and so on).⁴³ tDMRG methods combine these time integrators with the advantages of the MPS framework (such as the efficient truncation of quantum states, separate treatment of local sites and so forth).

If we ignore the special localised structure of the MPS/MPO representation and apply time evolution to the compressed MPS wave function directly, several global time-integration solvers can be implemented easily. For instance, the MPS can be updated via 4th-order Runge-Kutta method (for time-independent \hat{H}),

$$|K_1\rangle = -\frac{i\delta t}{\hbar}\hat{H}|\psi(t)\rangle, \quad (17)$$

$$|K_2\rangle = -\frac{i\delta t}{\hbar}\hat{H}(|\psi(t)\rangle + \frac{1}{2}|K_1\rangle), \quad (18)$$

$$|K_3\rangle = -\frac{i\delta t}{\hbar}\hat{H}(|\psi(t)\rangle + \frac{1}{2}|K_2\rangle), \quad (19)$$

$$|K_4\rangle = -\frac{i\delta t}{\hbar}\hat{H}(|\psi(t)\rangle + |K_3\rangle), \quad (20)$$

$$|\psi(t + \delta t)\rangle = |\psi(t)\rangle + \frac{1}{6}(|K_1\rangle + 2|K_2\rangle + 2|K_3\rangle + |K_4\rangle). \quad (21)$$

The Krylov subspace methods were also applied for the time-evolution of MPS, namely the global Krylov method (for a detailed discussion, see ref.²⁸). The order- r Krylov subspace generated by a Hamiltonian \hat{H} and an initial state $|\psi\rangle$ is the linear subspace spanned by images of $|\psi\rangle$ under the first r power of \hat{H} ,

$$\mathcal{K}_r(\hat{H}, |\psi\rangle) = \text{span}\{|\psi\rangle, \hat{H}|\psi\rangle, \dots, \hat{H}^r|\psi\rangle\}. \quad (22)$$

After orthonormalization of the subspace in Eq. 22, we could compute the exact \hat{U}' in this subspace and the projector \hat{P}_r onto orthonormalized \mathcal{K}_r , and the updated MPS is given by

$$|\psi(t + \delta t)\rangle \simeq \hat{P}_r^\dagger \hat{U}' \hat{P}_r |\psi(t)\rangle. \quad (23)$$

The global methods have the advantage of nearly exactly representing the operation of high-order Hamiltonian as $\hat{H}^n|\psi\rangle$, however they may become inefficient for large complicated systems

because of the much larger entanglement of the intermediate states (e.g. $|K_i\rangle$ in Eq. 17-20 and $\hat{H}^i|\psi\rangle$ in Eq. 22), which requires a much larger bond dimension. To overcome this bottleneck, the second advantage of the MPS framework (the existence of localised tensor components of MPS and MPO) can be put to use by considering local time evolution steps.

The Trotter-based methods^{19–23} is among the tDMRG methods working locally by splitting the total Hamiltonian \hat{H} into localised terms $\hat{H}_1, \hat{H}_2, \dots, \hat{H}_n$. Then the first-order TEBD propagation operator is expressed as

$$\hat{U}(t, t + \delta t) = e^{-i\sum_j \hat{H}_j(t)\delta t/\hbar} \simeq \prod_j e^{-i\hat{H}_j(t)\delta t/\hbar}. \quad (24)$$

Because of the local characteristic of each \hat{H}_j , the MPO form of $e^{-i\hat{H}_j(t)\delta t/\hbar}$ can be constructed easily. Trotter-based methods are very efficient for short range interaction systems due to the small number of terms while it is not efficient for systems containing many long range interaction terms.

Another important local method is the TDVP method^{30–32}. The basic idea of the TDVP method is very simple and based on

$$\min_{|\psi(t)\rangle} \|\hat{H}|\psi(t)\rangle - i\hbar \frac{\partial}{\partial t} |\psi(t)\rangle\|^2, \quad (25)$$

which is the variational version of TDSE (the Dirac-Frenkel principle); $\mathcal{F}(t) = \|\hat{H}|\psi(t)\rangle - i\hbar \frac{\partial}{\partial t} |\psi(t)\rangle\|^2$ is the Dirac-Frenkel functional.

With the MPS framework, the problem in Eq. 25 gets reduced to the minimization of Dirac-Frenkel functional $\mathcal{F}(t)$ with respect to the tensor components of the MPS. This can be achieved by projecting $\hat{H}|\psi(t)\rangle$ onto the tangent space of the given $|\psi(t)\rangle$ in the tensor manifold. The projector on the tangent space $\hat{P}_{T,|\psi(t)\rangle}$ is defined as

$$\hat{P}_{T,|\psi(t)\rangle} = \sum_{i=1}^n \hat{P}_{i-1}^L \otimes \hat{I}_i \otimes \hat{P}_{i+1}^R - \sum_{i=1}^{n-1} \hat{P}_i^L \otimes \hat{P}_{i+1}^R, \quad (26)$$

where \hat{P}_i^L (\hat{P}_i^R) is the left (right) block projector,

$$\hat{P}_i^L = \sum_{\alpha_i} |\mathcal{L}_{\alpha_i}^{[1:i]}\rangle \langle \mathcal{L}_{\alpha_i}^{[1:i]}|, \quad (27)$$

$$\hat{P}_i^R = \sum_{\alpha_i} |\mathcal{R}_{\alpha_i}^{[i:n]}\rangle \langle \mathcal{R}_{\alpha_i}^{[i:n]}|. \quad (28)$$

The original TDSE is then rewritten in a local version by inserting the projector (Eq. 26) on both sides of the original TDSE equation

$$i\hbar \frac{\partial}{\partial t} |\psi(t)\rangle = \hat{P}_{T,|\psi(t)\rangle} \hat{H} |\psi(t)\rangle. \quad (29)$$

Eq 29 can be solved approximately by solving n forward-evolving equations,

$$i\hbar \frac{\partial}{\partial t} |\psi(t)\rangle = \sum_{i=1}^n \hat{P}_{i-1}^L \otimes \hat{1}_i \otimes \hat{P}_{i+1}^R \hat{H} |\psi(t)\rangle, \quad (30)$$

and $n - 1$ backward-evolving equations,

$$i\hbar \frac{\partial}{\partial t} |\psi(t)\rangle = - \sum_{i=1}^{n-1} \hat{P}_i^L \otimes \hat{P}_{i+1}^R \hat{H} |\psi(t)\rangle. \quad (31)$$

In practice, Eq.30 and 31 are solved in the sequence defined by the order of the local sites. Here we take the one-site TDVP (1TDVP) method as an example: we start from $i = 1$ with a right-canonical form of the initial MPS, evolve the tensor component $A_{\alpha_{i-1}, \alpha_i}^{\sigma_i}$ based on the i -th term of the right hand side of Eq. 30, then left-orthonormalize the updated $\mathbf{A}^{\sigma_i} = \mathbf{L}^{\sigma_i} \mathbf{Q}^i$, evolve Q_{α_i, α_i}^i backward based on Eq. 31 before absorbing it into the next tensor component $\mathbf{A}^{\sigma_{i+1}} = \mathbf{Q}^i \mathbf{R}^{\sigma_{i+1}}$. We then repeat these steps for $i = i + 1$ to complete a left-to-right sweeping procedure. The two-site TDVP (2TDVP) follows a similar procedure.

B. Electron-vibration interaction model

Electron-vibration (el-vib) interaction models are used widely for the study of the non-adiabatic dynamics of organic molecular systems with ultrafast features and electron-nuclear interaction, e.g. the S_1/S_2 spectrum issue of pyrazine and the singlet fission (SF) in organic crystalline system which will be discussed in section III.

With a second-order truncation, the Hamiltonian for an el-vib coupled system can be expressed as

$$\hat{H} = \hat{H}_{el} + \hat{H}_{vib} + \hat{H}_{el-vib}, \quad (32)$$

with

$$\hat{H}_{el} = \sum_i \epsilon_i^0 |\psi_i\rangle \langle \psi_i| + \sum_{i \neq j} V_{ij}^0 |\psi_i\rangle \langle \psi_j|, \quad (33)$$

$$\hat{H}_{vib} = \sum_I \frac{1}{2} \hbar \omega_I \left(-\frac{\partial^2}{\partial Q_I^2} + Q_I^2 \right), \quad (34)$$

$$\hat{H}_{el-vib} = \sum_{i,j,I} g_{ij}^I Q_I |\psi_i\rangle \langle \psi_j| + \sum_{i,j,I,J} g_{ij}^{IJ} Q_I Q_J |\psi_i\rangle \langle \psi_j|. \quad (35)$$

Here, ϵ_i^0 and V_{ij}^0 represent the energy of the electronic state $|\psi_i\rangle$ and the electronic coupling between $|\psi_i\rangle$ and $|\psi_j\rangle$ under the equilibrium geometry respectively. ω_I is the frequency of the vibration mode I while Q_I is the dimensionless displacement. In the el-vib coupling, g_{ii}^I are linear local el-vib couplings and g_{ij}^I ($i \neq j$) are non-local ones; g_{ij}^{IJ} are the 2nd-order terms.

Considering the discrete basis and matrix representation of Hamiltonian using the MPS/MPO language, the second quantization is convenient for the tDMRG applications, and the three terms can be rewritten as

$$\hat{H}_{el} = \sum_i \epsilon_i^0 \hat{a}_i^\dagger \hat{a}_i + \sum_{i \neq j} V_{ij}^0 \hat{a}_i^\dagger \hat{a}_j, \quad (36)$$

$$\hat{H}_{vib} = \sum_I \hbar \omega_I (\hat{b}_I^\dagger \hat{b}_I + \frac{1}{2}), \quad (37)$$

$$\hat{H}_{el-vib} = \sum_{i,j,I} g_{ij,I}^I \hat{q}_I \hat{a}_i^\dagger \hat{a}_j + \sum_{i,j,I} g_{ij,I}^{II} \hat{q}_I \hat{q}_I \hat{a}_i^\dagger \hat{a}_j. \quad (38)$$

Here, \hat{a}_i^\dagger (\hat{a}_i) and \hat{b}_I^\dagger (\hat{b}_I) are the creators (annihilators) of electronic states $|\psi_i\rangle$ and vibration mode I respectively. $\hat{q}_I = \frac{1}{\sqrt{2}}(\hat{b}_I^\dagger + \hat{b}_I)$ is the dimensionless displacement operator of vibration mode I .

Obviously the occupation number representation of Bosonic states is the most convenient basis set for vibration sites. As the configuration number of this discrete basis is infinite, an effective basis truncation is necessary for the MPS and MPO construction. In our case, the basis set for a vibration site I is set to be $\{|0\rangle_I, |1\rangle_I, \dots, |n_{max}\rangle_I\}$, where the maximal occupation number n_{max} is carefully chosen by testing the convergence of dynamics under changes of n_{max} .

III. RESULTS AND DISCUSSION

Two chemical systems are investigated via tDMRG methods. The first one is the S_1/S_2 inter-conversion dynamics of the pyrazine molecule system where two electronic states are coupled to 24 discrete vibration modes by local, nonlocal and 2nd-order el-vib couplings. The second one is the singlet fission in a molecular dimer with three electronic states affected by a continuous phonon bath. All tDMRG calculations are performed using the SyTen package, originally created by Claudius Hubig.^{44,45}

A. The S_1/S_2 dynamics of pyrazine system

As a well-defined benchmark model system, the S_1/S_2 pyrazine system coupled with 24 molecular vibration modes has been studied by many quantum dynamics methods^{35,37,46–52} for several decades. The potential energy surfaces of singlet states S_1 and S_2 states of pyrazine have been computed via *ab initio* quantum chemistry methods such as configuration interaction (CI)⁴⁹ and complete active space self-consistent field (CASSCF) methods⁴⁷, which allows us to build the

el-vib interaction Hamiltonian to investigate the dynamics of this system,

$$\hat{H} = \begin{pmatrix} -\Delta & 0 \\ 0 & \Delta \end{pmatrix} + \sum_{I=1}^{24} \hbar \omega_I (\hat{b}_I^\dagger \hat{b}_I + \frac{1}{2}) \\ + \sum_{I=1}^{24} \hat{q}_I \begin{pmatrix} g_1^I & g_{12}^I \\ g_{12}^{I,1} & g_2^I \end{pmatrix} + \sum_{I,J=1}^{24} \hat{q}_I \hat{q}_J \begin{pmatrix} g_1^{IJ} & g_{12}^{IJ} \\ g_{12}^{IJ} & g_2^{IJ} \end{pmatrix}.$$

$\Delta = (E_{S_2} - E_{S_1})/2$ represents the electronic terms and the parameters in vibration and el-vib interaction terms can be found in references^{48,49}.

First, we test the performance of three tDMRG methods for the simplest 4-modes (v6a, v1, v9a and v10 in reference⁴⁸) el-vib interaction models with different maximal occupation numbers n_{max} of vibration sites. The initial state is set as $|\psi(0)\rangle = |S_2\rangle \otimes |0\rangle_{v6a} \otimes |0\rangle_{v1} \otimes |0\rangle_{v9a} \otimes |0\rangle_{v10}$ and total simulation time is fixed at 120 fs. The results of electronic population and autocorrelation function $C(t) = \langle \psi(0) | \psi(t) \rangle$ are shown in Fig. 1.

The results of second-order Taylor expansion in Fig. 1 (a, b) illustrate a crashed simulation with the maximal occupation numbers of 10 for all 4 modes, which suggests that the 2nd-order Taylor expansion method is invalid for large systems due to the large truncation error and unconserved energy and norm. The results of the global Krylov method and the 2TDVP method are consistent with each other, but the 2TDVP method is more stable and less time-consuming than the global Krylov methods. 1TDVP doesn't work properly for this case (Fig 2) and will be discussed in the next paragraphs. Therefore, the 2TDVP method is applied in the following calculations. On the other hand, the maximal occupation number test in Fig. 1 shows that systems with smaller n_{max} give incorrect dynamics results at earlier times, which demonstrates the increasing relevance of high occupation number states in the basis of Bosonic modes for a faithful representation of the quantum state; relatively large local basis sets for the vibration sites are needed for tDMRG calculation with a given simulation time. We investigated the suitable maximal occupation number for each mode individually to minimize the size of total basis. We fixed the maximal occupation numbers at 24, 18, 10 and 18 for mode v6a, v1, v9a and v10.

With the chosen tDMRG method (the 2TDVP method) and maximal occupation number of each Bosonic site, we also test the different time interval and truncation approximation of the 2TDVP method for the balance of efficiency and accuracy. The results are given in Fig. 2. The time interval tests in Fig 2 (a, b) display very little variation in the time-evolution behaviour for results achieved with $\delta t \leq 20.0$ a.u.; the trajectory for $\delta t = 40.0$ a.u. time intervals show an evident

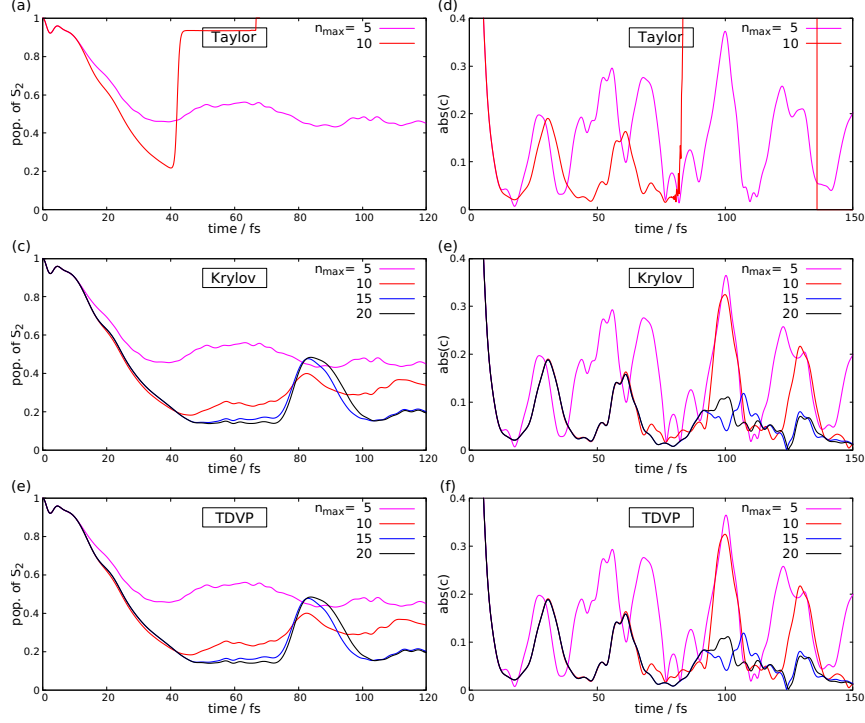


FIG. 1. The dynamics simulation tests of 4-modes pyrazine S_1/S_2 systems via (a, b) a 2nd-order Taylor expansion, (c, d) the Krylov method and (e, f) the 2-site TDVP method with different maximal occupation number of vibration sites. (a, c, d) show results of population evolution of S_2 and (b, d, f) give results of the absolute value of the autocorrelation function.

difference after about 50 fs. This suggests that the simulation time interval of pyrazine systems should be no larger than 20.0 a.u. (~ 0.48 fs).

As mentioned in Section II, the MPS can be truncated effectively to reduce computational cost. Generally, the truncation can be performed during the SVD steps occurring in the MPS construction and during the time evolution either by fixing the maximal number M of retained singular values (“maximum bond dimension”) or by discarding singular values below a fixed threshold ϵ . The latter one ensures a more even quality of simulation results and used here. Fig. 2 (c, d) illustrates the tests for 1TDVP and 2TDVP. The calculation using the non-truncating 1TDVP method is about 10 times faster than the truncated 2TDVP method but the former gives incorrect results after about 60 fs due to larger projecting error of 1TDVP method or the projection of the full TDSE with long-range interactions onto the MPS manifold of limited bond dimension. In other words, compared to 2TDVP, 1TDVP does not allow a sufficient adjustment of the effective basis and is exposed to problems of entanglement growth. Therefore, 1TDVP cannot yield reasonable

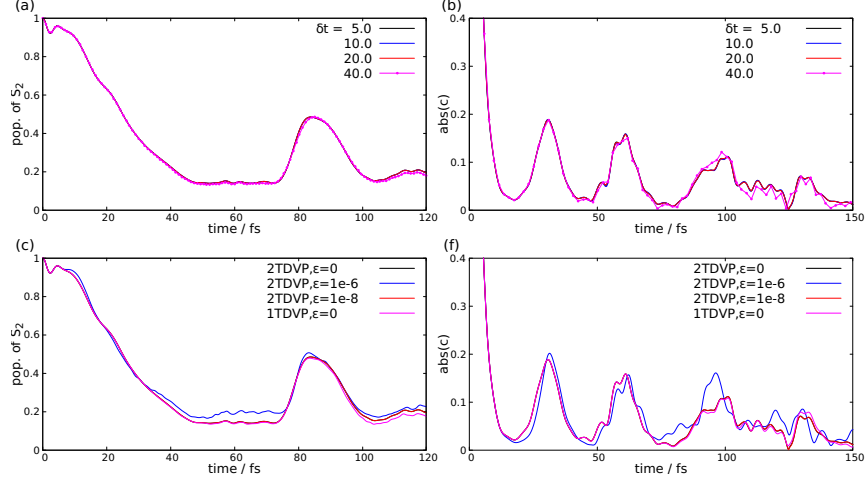


FIG. 2. The dynamics simulation tests of 4-mode pyrazine S_1/S_2 systems via the 2TDVP method. (a, b). The tests result of the population evolution of S_2 and the absolute value of autocorrelation function with different time intervals ($\delta t = 5.0, 10.0, 20.0$ and 40.0 a.u. respectively). (c, d). The test results for different truncations ϵ in 2TDVP.

results for realistic chemical systems. At the same time, we also notice from Fig. 2 (c, d) that 2TDVP with the truncation error threshold 1×10^{-8} gives nearly exact the same results with the non-truncating 2TDVP for the 4-mode pyrazine system, while 2TDVP with the truncation error threshold 1×10^{-6} still has visible deviations from the others.

The ordering of sites is another crucial issue for the performance of DMRG/tDMRG methods, a good ordering may lead to smaller bond dimension of MPO and MPS. We compare the time consumptions for the 4-mode system with seven different orderings by random selection and physical intuition of placing the highly correlated sites as close as possible. The results indicate that a proper ordering $\{v9a, v6a, |S_1\rangle, v10a, |S_2\rangle, v1\}$ based on the magnitude order of the el-vib couplings can be 10 times faster than the worst ordering $\{|S_1\rangle, v9a, v1, v6a, v10a, |S_2\rangle\}$ which puts the two electronic sites with small basis and large entanglement to other phonon modes the two ends of the chain. The results verify that the ordering of local sites will affect the efficiency of tDMRG calculation significantly and an optimal ordering should arrange sites with large interactions to be close to each other and locate the entangled sites with small basis at the center of the chain.^{53,54}

Based on the conclusions of the above tests, the parameters of the 2TDVP method were optimized to speed up the performance and the 2TDVP method was then applied to two 4/24-mode

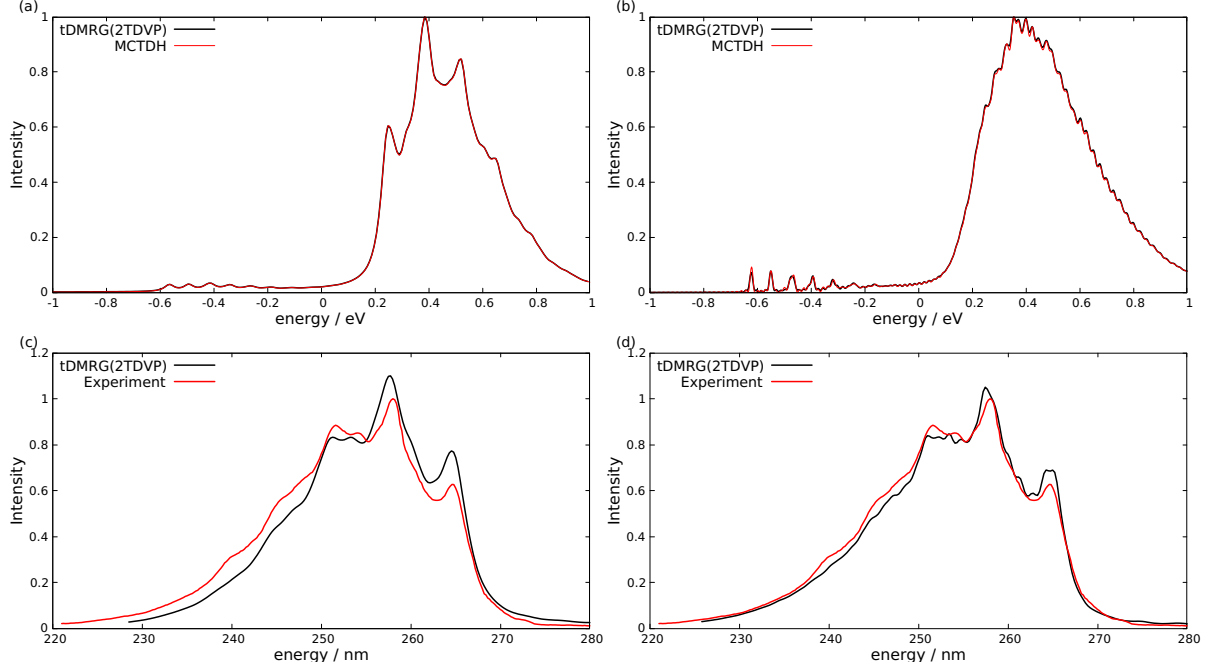


FIG. 3. Results for the spectra of the molecule pyrazine. (a) Spectrum (black line) of the 4-mode model with parameters in reference⁴⁸ comparing to MCTDH simulation (red line) result ($\tau = 30$ fs). (b) Spectrum (black line) of the 24-mode model with parameters as given in reference⁴⁸, compared to a MCTDH simulation (red line) result ($\tau = 30$ fs). (c) Spectrum (black line) of the 4-modes model with parameters as in reference⁴⁹ compared to experimental results⁵⁵ (red line) result ($\tau = 30$ fs). (d) Spectrum (black line) of the 24-mode model with parameters as in reference⁴⁹ compared to experimental results⁵⁵ (red line) result ($\tau = 50$ fs).

model systems^{48,49} of the pyrazine molecule. By calculating the Fourier transform of the product of the autocorrelation function $C(t)$ and a damping function $f(t) = e^{-|t|/\tau}$, the spectrum of the pyrazine system was obtained. The results for the spectrum are shown in Fig. 3. The results of the linearly approximated models are in good agreement with the results of the MCTDH method⁴⁸ in Fig 3 (a, b) and the results for second-order models⁴⁹ are comparable to experimental results⁵⁵. This nice agreement indicates that tDMRG is a feasible and accurate method for describing the quantum dynamics of realistic chemical systems. Furthermore, the time-evolution of bond dimension of are examined and we find that the bond-dimension m grows from 1 to around 1000 at 90 fs for this 24-mode system with $\varepsilon = 1 \times 10^{-8}$ (Fig 3 (d)) due to the entanglement growth during the time evolution.

TABLE I. The parameters of the SF electronic Hamiltonian matrix as in ref.⁶³. (unit: eV)

	LE	TT	CT
LE	0.10	0.00	-0.05
TT	0.00	0.00	-0.05
CT	-0.05	-0.05	0.30

B. Singlet fission in a molecular dimer

The singlet fission (SF) is a spin-allowed photophysical process that splits one singlet excitation state into two triplet excitons in various organic materials.^{56–58} It is generally assumed that there are three crucial groups of electronic states for singlet fission, namely local excitation (LE) states, charge transfer (CT) states and triplet pair (TT) states. Many experimental and theoretical studies of SF have indicated that vibration modes play very important roles for SF^{59–62}, but the full quantum treatment of both the electronic and vibrational part is still challenging because of the large configuration space of many electronic states and many vibration or phonon modes.

Here we test the tDMRG dynamics of the SF, comparing our results to a recent ML-MCTDH simulation by Lan et al.⁶³. For this, we adopt the model used in ref.⁶³ which contains three electronic states (one LE state, one CT state and one TT state) and a linear local el-vib coupling approximation (i.e. $g_{ij}^{II} = 0$ and $g_{ij}^I = 0(i \neq j)$). The parameters for the electronic part are listed in Tab I.

The vibration and el-vib interaction terms are characterized by the continuous Debye-type spectral density

$$J_i(\omega) = \frac{2\lambda\omega\omega_0}{\omega^2 + \omega_0^2}, \quad (39)$$

where $\lambda = 0.1$ eV represents the strength of the el-vib coupling and $\omega_0 = 0.18$ eV is the characteristic frequency of the bath. i is the index for three electronic states. Consequently, the local el-vib couplings can be computed by discretizing the spectral density

$$g_i^I = \sqrt{\frac{2}{\pi} J_i(\omega_I) \Delta\omega_I} \quad (40)$$

with a discrete series of bath frequencies $\{\omega_I\}$ in a given region and $\Delta\omega_I = \omega_I - \omega_{I-1}$.

First, the relevant region of the spectral density (0-0.4 eV) is separated into eight regions following reference⁶³, namely 0-0.075 eV (R1), 0.075-0.108 eV (R2), 0.108-0.125 eV (R3), 0.125-

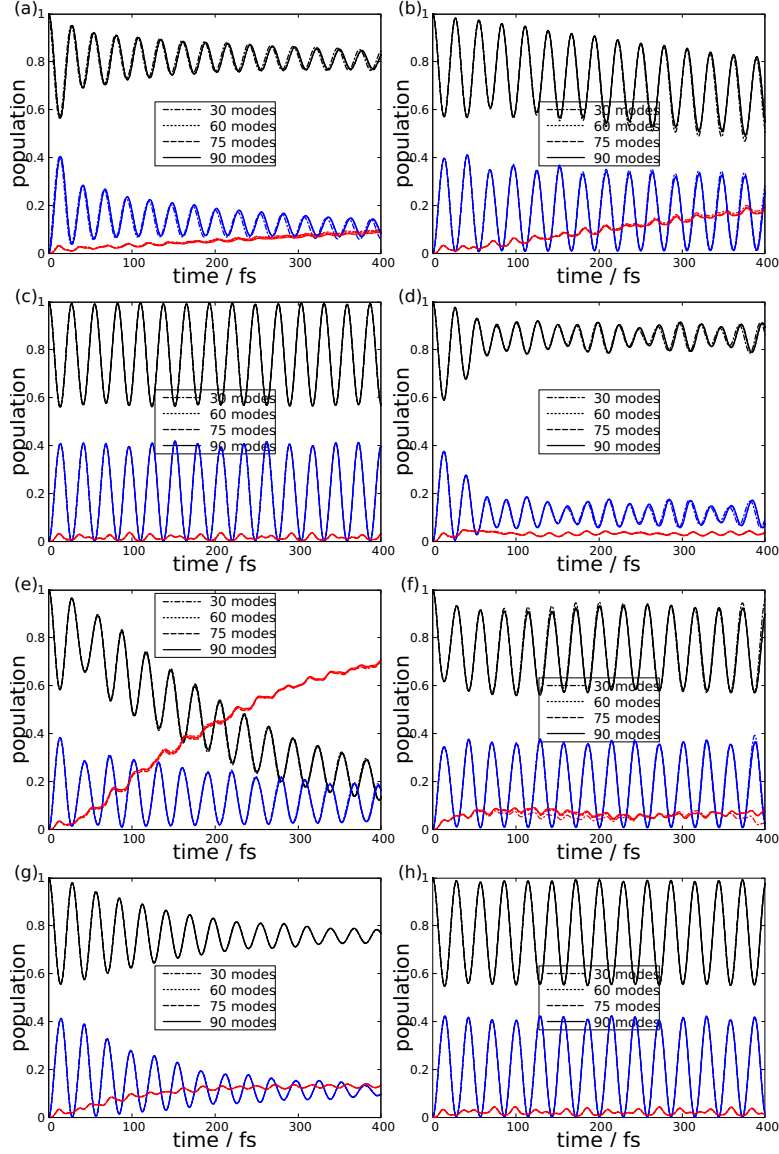


FIG. 4. The time-evolution for the populations of three electronic states (LE state with black lines, CT state with blue lines and TT state with red lines) for the SF dynamics with the bath in specific energy regions of (a) 0-0.075 eV (R1), (b) 0.075-0.108 eV (R2), (c) 0.108-0.125 eV (R3), (d) 0.125-0.165 eV (R4), (e) 0.165-0.2 eV (R5), (f) 0.2-0.3 eV (R6), (g) 0.3-0.35 eV (R7) and (h) 0.35-0.4 eV (R8). Different numbers of modes are used to test the convergence of the representation of the continuous vibration bath.

0.165 eV (R4), 0.165-0.2 eV (R5), 0.2-0.3 eV (R6), 0.3-0.35 eV (R7) and 0.35-0.4 eV (R8), to investigate the effects of bath modes in different energy ranges. The issue of bath representation convergence is tested by increasing the number of discrete vibration modes (10, 20, 25 and 30 modes for each electronic states in all eight regions). The results are illustrated in Fig. 4. The

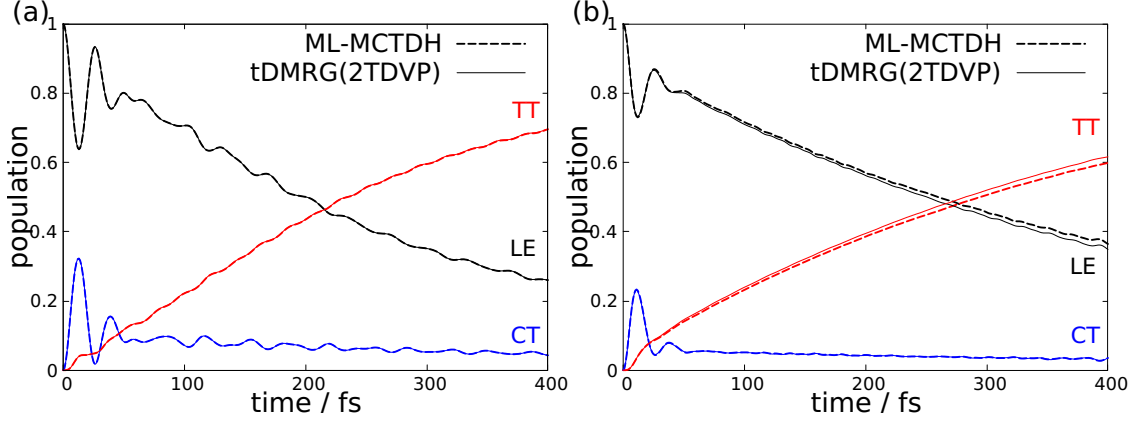


FIG. 5. The time-evolution for the populations of three electronic states of the SF dynamics coupled to the bath in the energy regions of (a) R4 + R5 + R7 (90 modes) and (b) 0-0.4 eV (183 modes) by tDMRG (solid lines) and ML-MCTDH (dash lines)⁶³.

converged results of the electronic population evolution show good agreement with Lan et al.'s ML-MCTDH simulation. Our results with different numbers of discrete modes in regions R3, R4, R7 and R8 show very quick convergence while R1, R2, R5 and R6 require much larger number of vibration modes to converge the dynamics.

The population results in Fig 4 clearly indicate that the phonon modes in energetic ranges R4, R5 and R7 play the most important roles influencing the SF dynamics. The coupling to the bath modes in regions R4 and R7 decreases the oscillation amplitudes of the LE and CT populations significantly (Fig 4(d, g)) while the TT state of SF is ultrafast formed mainly due to the effect of the coupling to the bath in range R5 (Fig 4(e)). Therefore, the dynamics of SF accounting for the effects of the bath may be simulated approximately by including the three vibration regions R4, R5 and R7. We also calculate the dynamics of the SF system in the case where all eight domains of the bath are included, compared to the reduced bath (R4, R5, R7).⁶³ Our population dynamics results with energy windows as displayed in Fig. 5 are in very good agreement with the ML-MCTDH simulation in ref.⁶³, showing again that tDMRG can be used for the accurate and efficient simulation of quantum dynamics in large chemical systems.

IV. SUMMARY

In order to validate the accuracy and efficiency of various tDMRG methods for realistic electron-vibration/phonon systems, we benchmarked the tDMRG calculations with different algo-

gorithms (global Taylor, global Krylov, local 1TDVP and 2TDVP) for the S_1/S_2 internal conversion in the pyrazine molecule and applied a TDVP calculation to the singlet fission in a molecular dimer. Our tDMRG results were compared with (ML-)MCTDH and experimental results.

We find that time-evolution of large systems via 2nd-order Taylor expansion may crash due to its large truncation error of time evolution propagator \hat{U} with respect to the system size while local methods (e.g. TDVP methods) give reasonable results. Between two TDVP methods (one- and two-site TDVP), 2TDVP performs better than 1TDVP for realistic chemical systems because it gives less projecting error especially for systems with long range interaction. Furthermore, several key parameters in the tDMRG calculation including the truncation error threshold, time interval and ordering of local sites were investigated to strike the balance between efficiency and accuracy of results. It is worthwhile to emphasize that the ordering of sites will be a very important factor influencing the efficiency of TDVP methods. We suggest to arrange strongly correlated sites close to each other and locate the entangled sites with small basis at the center of the chain.

The comparison of dynamics results of optimized tDMRG simulations to the benchmarks of (ML-)MCTDH and experimental results for both systems confirms that the tDMRG methods (particularly, the 2TDVP method) are good candidates for quantum dynamics calculations for chemical systems. Our tests provide guidelines for future applications of tDMRG methods to simulate quantum dynamics of realistic chemical systems.

V. ACKNOWLEDGMENTS

The work was supported by the National Natural Science Foundation of China (Grant Nos. 21722302 and 21673109) and by the Deutsche Forschungsgemeinschaft (DFG, German Research Foundation) under Germanys Excellence Strategy—EXC-2111—No. 390814868. We thank Victor S. Batista, Claudius Hubig, Zhenggang Lan, Sam Mardazad, and Yu Xie for helpful discussions.

REFERENCES

- ¹T. G. Kolda and B. W. Bader, SIAM Rev. **51**, 455 (2009).
- ²S. Dolgov, *Tensor product methods in numerical simulation of high-dimensional dynamical problems*, Ph.D. thesis, University of Leipzig (2014).

- ³L. R. Tucker, *Psychometrika* **31**, 279 (1966).
- ⁴H.-D. Meyer, U. Manthe, and L. S. Cederbaum, *Chem. Phys. Lett.* **165**, 73 (1990).
- ⁵M. H. Beck, A. Jäckle, G. A. Worth, and H.-D. Meyer, *Phys. Rep.* **324**, 1 (2000).
- ⁶L. De, B. De Moor, and J. Vandewalle, *SIAM J. Matrix Anal. Appl.* **21**, 1324 (2000).
- ⁷L. De Lathauwer, B. De Moor, and J. Vandewalle, *SIAM J. Matrix Anal. Appl.* **21**, 1253 (2000).
- ⁸H. Wang and M. Thoss, *J. Chem. Phys.* **119**, 1289 (2003).
- ⁹I. V. Oseledets, *SIAM J. Sci. Comput.* **33**, 2295 (2011).
- ¹⁰F. Verstraete, V. Murg, and J. I. Cirac, *Adv. Phys.* **57**, 143 (2008).
- ¹¹U. Schollwöck, *Ann. Phys.* **326**, 96 (2011).
- ¹²S. R. White, *Phys. Rev. Lett.* **69**, 2863 (1992).
- ¹³U. Schollwöck, *Rev. Mod. Phys.* **77**, 259 (2005).
- ¹⁴F. Verstraete and J. I. Cirac, arXiv preprint cond-mat/0407066 (2004).
- ¹⁵Y.-Y. Shi, L.-M. Duan, and G. Vidal, *Phys. Rev. A* **74**, 022320 (2006).
- ¹⁶N. Nakatani and G. K.-L. Chan, *J. Chem. Phys.* **138**, 134113 (2013).
- ¹⁷K. Gunst, F. Verstraete, S. Wouters, O. Legeza, and D. Van Neck, *J. Chem. Theory Comput.* **14**, 2026 (2018).
- ¹⁸F. A. Schröder, D. H. Turban, A. J. Musser, N. D. Hine, and A. W. Chin, *Nat. Commun.* **10**, 1062 (2019).
- ¹⁹S. R. White and A. E. Feiguin, *Phys. Rev. Lett.* **93**, 076401 (2004).
- ²⁰A. J. Daley, C. Kollath, U. Schollwöck, and G. Vidal, *J. Stat. Mech.: Theory Exp.* **2004**, P04005 (2004).
- ²¹F. Verstraete, J. J. Garcia-Ripoll, and J. I. Cirac, *Physical review letters* **93**, 207204 (2004).
- ²²G. Vidal, *Phys. Rev. Lett.* **91**, 147902 (2003).
- ²³G. Vidal, *Phys. Rev. Lett.* **93**, 040502 (2004).
- ²⁴M. Suzuki, *Commun. Math. Phys.* **51**, 183 (1976).
- ²⁵E. Ronca, Z. Li, C. A. Jimenez-Hoyos, and G. K.-L. Chan, *J. Chem. Theory Comput.* **13**, 5560 (2017).
- ²⁶J. Ren, Z. Shuai, and G. Kin-Lic Chan, *J. Chem. Theory Comput.* **14**, 5027 (2018).
- ²⁷L.-H. Frahm and D. Pfannkuche, *J. Chem. Theory Comput.* **15**, 2154 (2019).
- ²⁸S. Paeckel, T. Köhler, A. Swoboda, S. R. Manmana, U. Schollwöck, and C. Hubig, arXiv preprint arXiv:1901.05824 (2019).
- ²⁹J. J. García-Ripoll, *New J. Phys.* **8**, 305 (2006).

- ³⁰J. Haegeman, J. I. Cirac, T. J. Osborne, I. Pižorn, H. Verschelde, and F. Verstraete, Phys. Rev. Lett. **107**, 070601 (2011).
- ³¹C. Lubich, I. V. Oseledets, and B. Vandereycken, SIAM J. Numer. Anal. **53**, 917 (2015).
- ³²J. Haegeman, C. Lubich, I. Oseledets, B. Vandereycken, and F. Verstraete, Phys. Rev. B **94**, 165116 (2016).
- ³³Y. Kurashige, J. Chem. Phys. **149**, 194114 (2018).
- ³⁴Q. Shi, Y. Xu, Y. Yan, and M. Xu, J. Chem. Phys. **148**, 174102 (2018).
- ³⁵S. M. Greene and V. S. Batista, J. Chem. Theory Comput. **13**, 4034 (2017).
- ³⁶Y. Yao, K.-W. Sun, Z. Luo, and H. Ma, J. Phys. Chem. Lett. **9**, 413 (2018).
- ³⁷A. Baiardi and M. Reiher, J. Chem. Theory Comput. **15**, 3481 (2019).
- ³⁸W. Li, J. Ren, and Z. Shuai, arXiv preprint arXiv:1907.12044 (2019).
- ³⁹H. Ma, Z. Luo, and Y. Yao, Mol. Phys. **116**, 854 (2018).
- ⁴⁰H. Tal-Ezer and R. Kosloff, J. Chem. Phys. **81**, 3967 (1984).
- ⁴¹O. Nevanlinna, *Convergence of iterations for linear equations* (Birkhäuser, 2012).
- ⁴²Y. Saad, *Iterative methods for sparse linear systems*, Vol. 82 (siam, 2003).
- ⁴³C. Moler and C. Van Loan, SIAM Rev. **45**, 3 (2003).
- ⁴⁴C. Hubig, F. Lachenmaier, N.-O. Linden, T. Reinhard, L. Stenzel, A. Swoboda, and M. Grundner, “The SYTEN toolkit,” .
- ⁴⁵C. Hubig, *Symmetry-Protected Tensor Networks*, Ph.D. thesis, LMU München (2017).
- ⁴⁶L. Seidner, G. Stock, A. Sobolewski, and W. Domcke, J. Chem. Phys. **96**, 5298 (1992).
- ⁴⁷C. Woywod, W. Domcke, A. L. Sobolewski, and H.-J. Werner, J. Chem. Phys. **100**, 1400 (1994).
- ⁴⁸G. A. Worth, H.-D. Meyer, and L. Cederbaum, J. Chem. Phys. **105**, 4412 (1996).
- ⁴⁹A. Raab, G. A. Worth, H.-D. Meyer, and L. Cederbaum, J. Chem. Phys. **110**, 936 (1999).
- ⁵⁰I. Burghardt, K. Giri, and G. Worth, J. Chem. Phys. **129**, 174104 (2008).
- ⁵¹M. A. Saller and S. Habershon, J. Chem. Theory Comput. **11**, 8 (2014).
- ⁵²B. Kloss, I. Burghardt, and C. Lubich, J. Chem. Phys. **146**, 174107 (2017).
- ⁵³T. Xiang, Physical Review B **53**, R10445 (1996).
- ⁵⁴Ö. Legeza and J. Sólyom, Physical Review B **68**, 195116 (2003).
- ⁵⁵I. Yamazaki, T. Murao, T. Yamanaka, and K. Yoshihara, Faraday Disc. Chem. Soc. **75**, 395 (1983).
- ⁵⁶M. B. Smith and J. Michl, Chem. Rev. **110**, 6891 (2010).
- ⁵⁷M. B. Smith and J. Michl, Annu. Rev. Phys. Chem. **64**, 361 (2013).

- ⁵⁸D. Casanova, Chem. Rev. **118**, 7164 (2018).
- ⁵⁹Y. Yao, Phys. Rev. B **93**, 115426 (2016).
- ⁶⁰K. Miyata, Y. Kurashige, K. Watanabe, T. Sugimoto, S. Takahashi, S. Tanaka, J. Takeya, T. Yanai, and Y. Matsumoto, Nat. Chem. **9**, 983 (2017).
- ⁶¹H. Zang, Y. Zhao, and W. Liang, J. Phys. Chem. Lett. **8**, 5105 (2017).
- ⁶²X. Xie, A. Santana-Bonilla, W. Fang, C. Liu, A. Troisi, and H. Ma, J. Chem. Theory Comput. **15**, 3721 (2019).
- ⁶³J. Zheng, Y. Xie, S. Jiang, and Z. Lan, J. Phys. Chem. C **120**, 1375 (2016).